Seismic monitoring of well integrity

D. W. Vasco[1], Thomas M. Daley[1], Verónica Rodríguez Tribaldos[1], Pierpaolo Marchesini[2], G. M. Hoversten[1], Gwyn Mali[3], Dimitri Bevc[4], and Valeri Korneev[1*]

1 Energy Geosciences Division, Lawrence Berkeley National Laboratory, University of California, Berkeley, CA

2 Silixa Ltd, London, UK

3 Chevron North America Exploration and Production Company, a division of Chevron U.S.A. Inc., Bakersfield, CA

4 Chevron Technical Center, a division of Chevron U.S.A. Inc., Houston, TX

Introduction

With approximately 1 million active oil and gas wells, and over 3 million abandoned wells in the United States alone, the issue of well integrity is an important one (Jackson 2014). This issue takes on greater significance with the predicted growth of carbon capture and storage, or sequestration (CCS). Such wells will be subject to complex chemical reactions and required to last for much longer than current oil wells. Given the immense number of existing wells and the large number of wells needed for effective CCS, it would be advantageous to have a quick and inexpensive technique for determining the state of a well. Seismic tube waves, produced by the flexure of the well itself, pressure changes in the fluid in the well, and the deformation of the material immediately surrounding the well, are particularly sensitive to variations in the state of the well and the near well environment (Hornby et al. 1989, Sinha and Kostek 1996, Simsek and Sinha 2008). For example, tube waves are routinely used in borehole logging tools to evaluate formation elastic properties. In spite of their sensitivity to the state of the borehole and its immediate surroundings, tube waves are not routinely used to determine the condition of a well.

In this paper we evaluated simple seismic methods for generating and observing tube waves as a means of detecting well damage. In particular, we explore using surface sources and receivers to detect tube waves that propagate the length of the well and reflect from the bottom of the well and return to the Earth's surface. Rather than solely describing our successes, this work describes the lessons learned in our monitoring efforts, and where improvement in needed in order to achieve the consistent results required for successful monitoring.

Methodology and Modeling

At the outset, the field work described below was exploratory in nature. The early objective was to visit both healthy and broken wells, excite and record seismic waves that propagate up and down the borehole and determine if there is any detectable difference in the response of the two classes of wells (healthy and broken).

Finite difference modeling

In order to understand the results of the experiments it is helpful to have a basic understanding of the seismic excitation of a well of finite length. To facilitate this, we conducted some numerical modeling to guide our field experiments. Because of the small strains, the propagation of the tube waves that we generated is governed by the elastodynamic equation of motion. The nature of the elastic waves is dominated by the boundary conditions of the interface between the fluid-filled well and the surrounding rock formation. We adopted a straightforward finite difference solution to the governing equations, assuming cylindrical symmetry around the well bore (thus elliptical boreholes are not allowed). This reduced the problem to two dimensions and made the numerical calculations for complex well completions tractable. Layering and variable borehole diameters are allowed, though the diameter could not be smaller than the radial grid spacing. However, this method did not allow for boreholes with elliptical cross-sections or the asymmetry that might occur in a bent well. However, the method did allow for the arbitrary variations in well properties with depth and radius that are needed to describe the well completions.

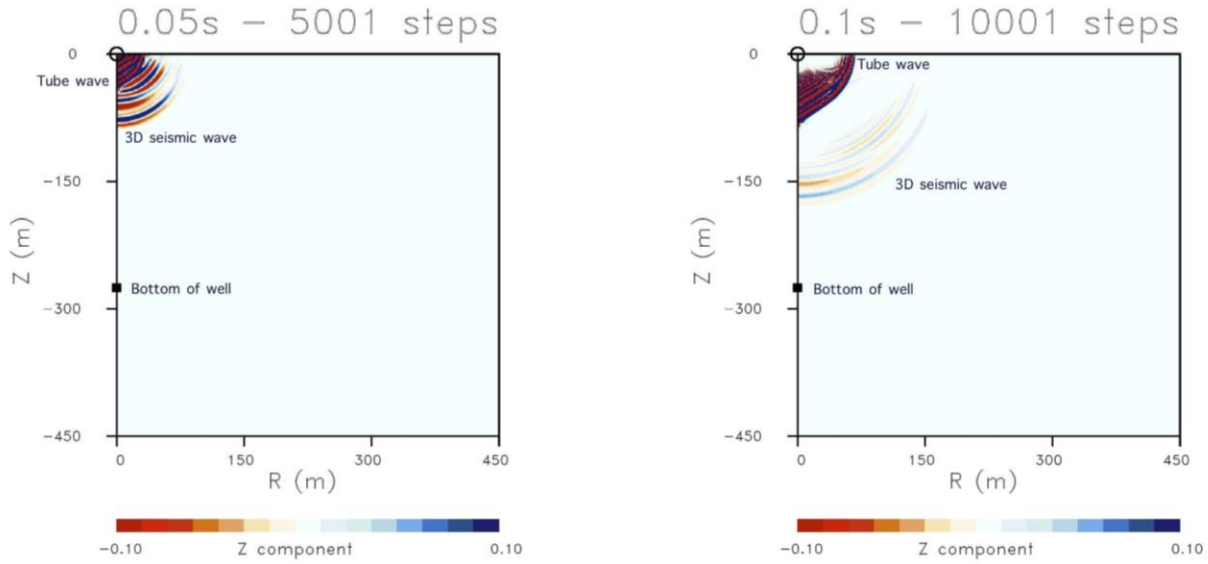

Figure 1. (Left) Wave field 0.05s after the activation of the source. The bottom of the well is indicated by the black square. (Right) Wavefield after 0.1s. The faint oscillations leading the tube wave field are the body waves propagating outward into the medium.

In the finite difference modeling we discretize the partial differential equation governing elastic wave propagation, representing the properties of the borehole and the surrounding medium on a grid. Assuming cylindrical symmetry we can represent the medium using a two-dimensional grid. In the simulations shown in this section we assume a water-filled well with a radius of 15 cm, surrounded by 1 cm thick steel casing. The compressional velocity of the surrounding medium is 1500 m/s and the shear velocity is 677 m/s, representative of the values at a field in California. A vertical point source is activated at the surface, exciting a range of seismic waves as shown in Figure 1.

Several types of waves are set in motion, including a pressure wave in the fluid, an interface wave at the boundary of the borehole, and an elastic wave that propagates outward into the elastic medium. Waves that propagate outward into the medium spread energy outward into three dimensions and decay more rapidly than waves that propagate along the borehole. For example, in the right panel of Figure 1 we observed that after 0.1s the body wave propagating outward into the medium is much smaller than the tube wave. With time, the body

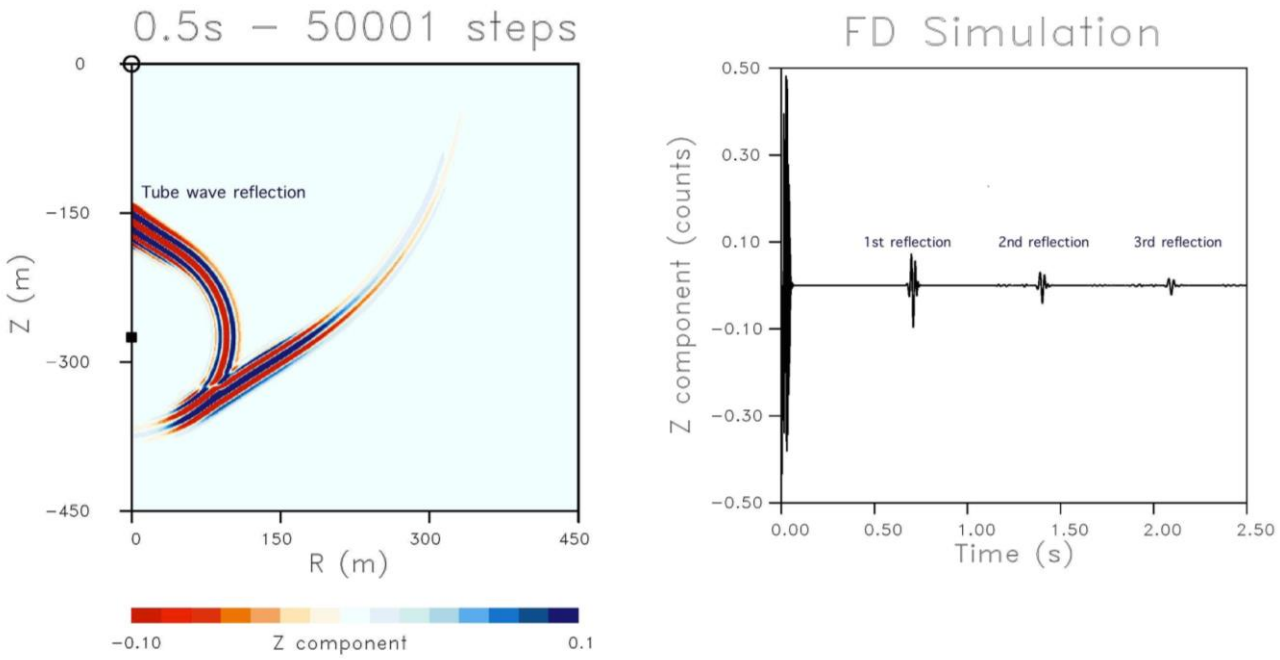

Figure 2. (Left) Wavefield after 0.5s. (Right) Seismic trace of the wave field recorded at the Earth's surface showing tube-wave refletions.

waves propagate away and we are left with the tube waves. Even though the tube waves are restricted to the boundary region of the well, they do generate elastic waves that propagate outward into the medium (Figure 2). As the tube wave reaches the bottom of the well it is reflected back up the well towards the surface, while the conical wave shed by the downward propagating tube wave continues out into the medium, this is shown in Figure 2. The reflected tube wave eventually reaches the surface where it may be recorded by a surface

seismometer. If the attenuation in the medium is low, the entire process may repeat itself for many cycles, leading to repeated tube wave reflections recorded at the surface. Typically, the waves attenuate significantly and one may only record a single reflection, or with high attenuation and a weak source, no reflection at all. The seismic wave field calculated for a seismometer at the surface is shown in right panel of Figure 2. In this panel one can see the initial source excitation followed by three tube-wave reflections from the bottom of the well, representing multiple trips along the length of the well. Thus, the main features of this simple model of an intact well are the energy due to the source followed by one or more tube wave reflections.

Field Experiments and Results

Now that we have some insight into the propagation of tube waves provided by the numerical modeling, we can consider actual field data from experiments conducted at two oil fields in California. For this project we conducted two sets of experiments.

First Field Test

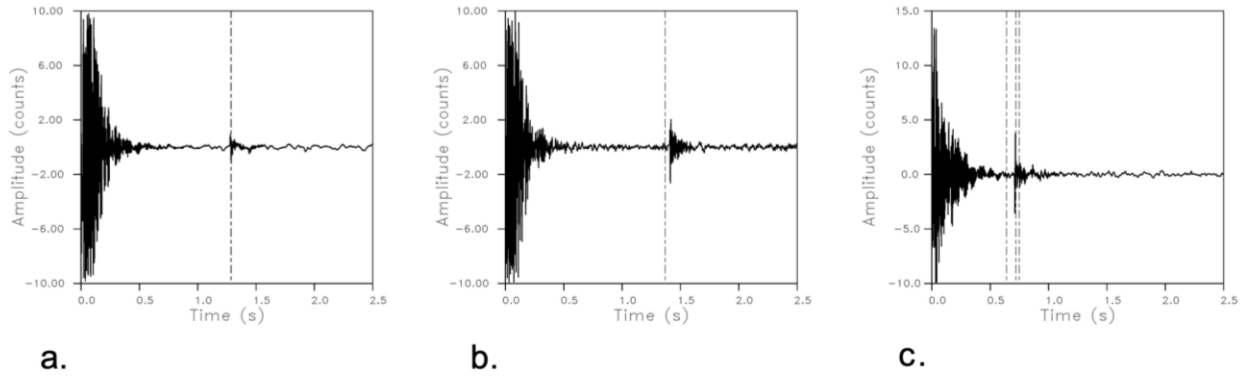

Figure 3. (a) Seismic trace for the first healthy well. (b) Seismic trace for the second healthy well. (c) Seismic trace for the third healthy that was tested. The dashed vertical lines indicate the times required for tube waves to propagate to the end of each well and back. In the third well the well termination was complicated, giving rise to three possible reflections.

In the first field campaign a total of five wells were examined, in an effort to see if there were differences between broken and healthy wells. The experiment is very simple, seismic sensors are attached to the well head and coupled to the ground near the well. A hammer was used to generate a coupled seismic wave, by both striking the well head and the ground adjacent to the well. The waves generated by the hammer blow, including all tube waves, are recorded by the seismometers. The digital recordings of the data were analyzed at Lawrence

Berkeley Laboratory, in an effort to discern differences between healthy and broken wells. Seismograms, recorded at the surface, for the three healthy wells are plotted in Figure 3.

For comparison, hammer tests were conducted at two broken wells. We plot seismograms associated with the two verified broken wells in Figure 4.

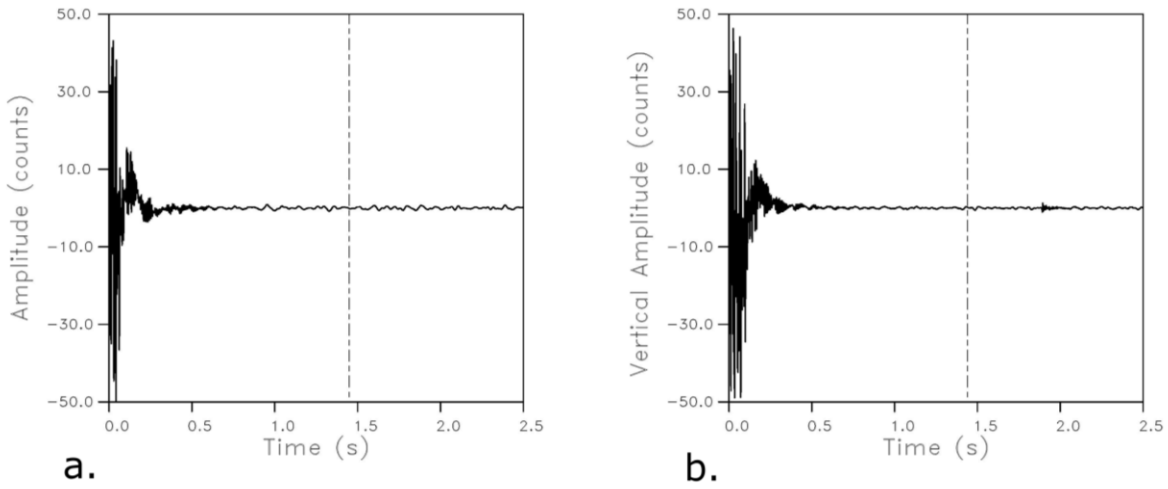

Figure 4. (a) Seismic trace for the first broken well. The dashed vertical line indicates the time required for the tube wave to propagate to the end of the well and back. (b) Seismic trace for the second broken well that was tested.

There are clear differences between the healthy and broken wells for the examples shown here. The healthy wells have significant arrivals at times that correspond to tube wave reflections off the bottom of the wells, much like the example given in the finite difference calculation. Such arrivals are not seen in the broken wells, suggesting that the damage might lead to changes in the well that attenuate or eliminate the propagating tube waves. We should note that each well was hit twenty times, ten strikes to the ground and ten to the well head. We could not get consistent results for each strike and many strikes did not show the secondary arrivals that we are associating with tube wave reflections. This variation may be an indication that our source was inadequate for generating sufficiently strong tube waves in a consistent fashion. One critical factor is the depth to the water column within the well. As shown in the crosswell results below, it is important to excite a strong oscillation in the fluid in order to generate robust tube waves. Still, the initial results were encouraging enough to attempt a more comprehensive study with many more wells.

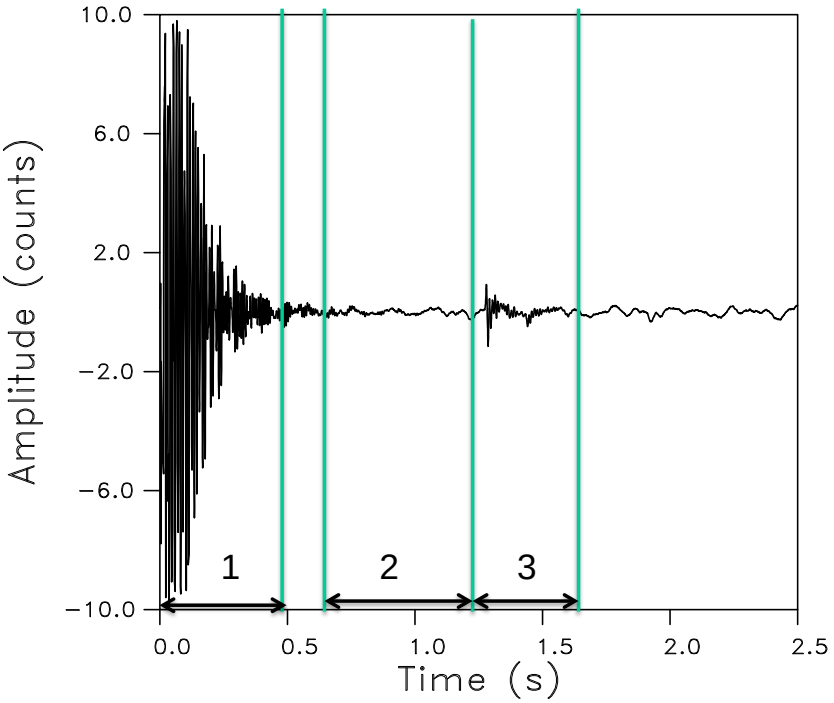

Figure 5. Seismic trace associated with the first healthy well, considered previously in Figure 3. Three distinct time windows are indicated by the vertical lines and the numbered segments. In the figures that follow, we will apply the Fourier transform to the time series in windows 1 and 3.

Second Field Test

The goal of the follow-up field test was to visit a larger suite of wells in order to verify the earlier results and gather a sufficient sampling of wells. Thus, in the second experiment we visited twenty wells and repeated the experiments. In this second set of examples, it also proved difficult to get consistent visible pulses that match secondary arrivals corresponding to reflected tube waves, even when a larger accelerated weight drop source was used. Again, this suggests that neither the hammer source nor the accelerated weight drop were sufficient to produce consistently large amplitude tube wave reflections that are visible above the ambient noise in the seismic traces.

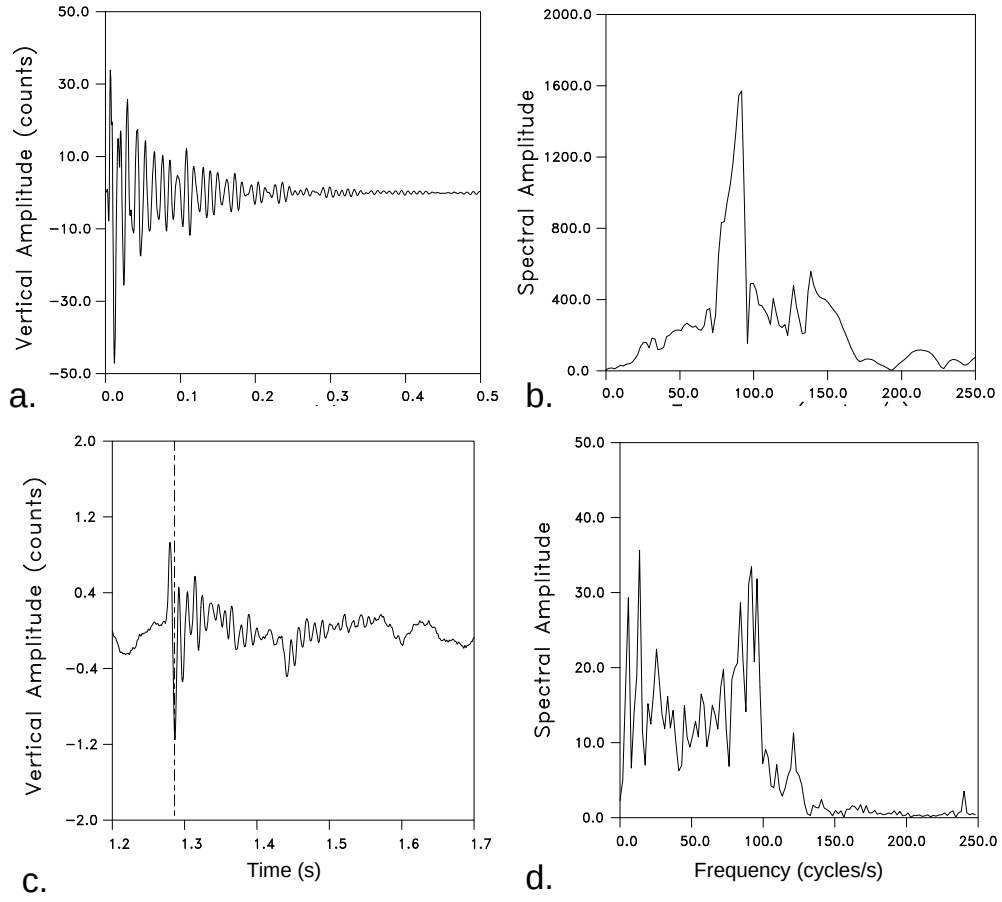

Figure 6. (a) Time series associated with the first time window in Figure 5. (b) Fourier transform of the time series in window 1. (c). Time series for the time window 3, indicated in Figure 5. (d). Spectral amplitude as a function of frequency for time window 3.

Therefore, for this second set of data we utilized more advanced frequency-domain techniques in order to detect differences between healthy and broken wells. As an example, let us consider the previous seismic trace associated with the first healthy well, shown in Figure 3a. If we partition the trace into three distinct segments, as shown in Figure 5, we can take the Fourier transform of the time series in each segment. Consider the first segment, number 1, containing the main wave field generated by striking the ground adjacent to the well (Figure 6a). The high amplitude seismic energy is due to the vibrations of the well head, as well as due to surface waves, and near field motion. The Fourier transform of this time series is plotted in Figure 6b. Next, consider the third and final time window in Figure 5, which contains the later arriving energy that comes in at the arrival time of the tube wave reflection from the bottom of the well (Figure 6c). The Fourier spectrum for this time interval is shown in Figure 6d.

The Fourier spectrum is a blend of the high frequency tube wave reflection and the lower frequency microseismic noise. Thus, it is possible to use the frequency content of segments of the trace to discriminate between microseismic noise and arrivals related to the excitation from the hammer blow. We can calculate the frequency spectrum for a window that moves along the trace. The result is a spectrum that varies over time, where the time indicates the center point of the time window. The example for the trace from the first healthy well is shown in Figure 7.

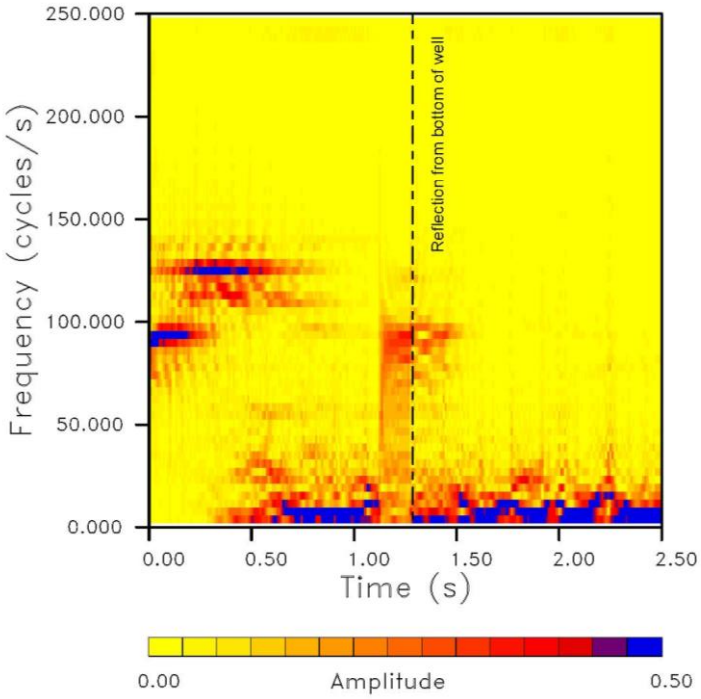

Figure 7. Frequency spectrum of the trace from the first healthy well, corresponding the trace plotted in Figure 5, as a function of time along the trace (time-frequency decomposition).

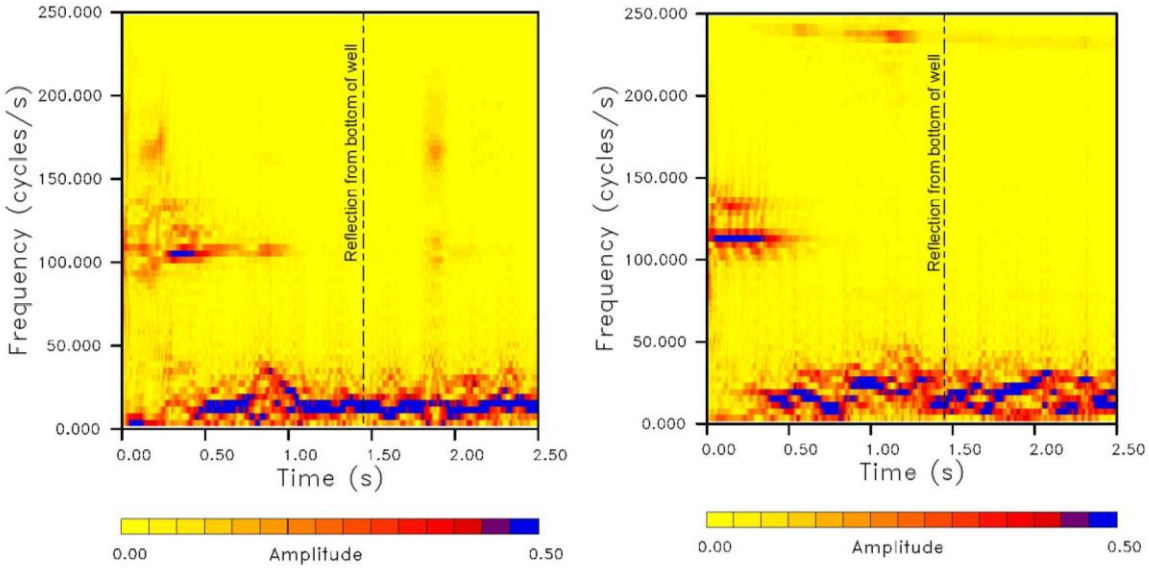

Figure 8. Frequency spectrum of the trace from the second broken well, shown in Figure 4, as a function of time along the trace (time-frequency decomposition). (Left panel) Current test. (Right panel) Previous test.

For the early times one sees the high frequency energy associated with the hammer blow. This is followed by lower energy content until about 1.25s when higher frequencies again appear, likely due to the arrival of the reflected tube wave. If there is sufficient frequency separation between the microseismic noise and the tube wave then the time-frequency decompositions could potentially discriminate between healthy and broken wells, even when we have not excited a tube wave that is strong enough to be clearly visible above the microseismic noise in time domain. In order to test this, we applied the time-frequency decomposition to the traces from all of the wells that we visited during the second field campaign.

First, we consider a broken well and we qualify the results because we do not know the exact nature of the trouble in each well. That is, while we have the completion diagrams for each well and we know the set of wells that are sufficiently distorted that a logging tool was unable to progress beyond a certain depth, we do not have caliper logs of the damaged wells. However, we hypothesized that, given sufficient damage, the expected tube wave reflection will be strongly attenuated or absent. In Figure 8 we present results for a broken well. This well was the second broken well examined during the first field campaign and revisited as a consistency check on the equipment and operation of the second field experiment. The two tests give similar results, indicating that our setup is consistent with the previous field test. The time-frequency analysis indicates that no high frequency energy appears after the initial hammer blow. In particular, there is no obvious energy when we predict that the tube wave reflection from the base of the well should occur. The time-frequency decomposition for the four other tests involving broken wells did not have high frequency energy following the initial signal due to the hammer strike. In particular, there was no high frequency energy appearing at the time associated with the reflection of the tube wave from the bottom of the well.

We can compare the findings for broken wells with the response of a healthy well to the hammer blows. As an example, consider the results for a competent well, plotted in Figure 9. In this well one observes energy following the high frequency vibrations due to the hammer strike. The slight peak in energy appears at the predicted arrival time of the reflected tube wave. We should emphasize that, although the secondary peak is subtle, it does occur for all the hammer strikes that we conducted for each well test. That is, unlike the results from the first set of experiments, this secondary peak is consistent across all strikes at a given well. For example, in Figure

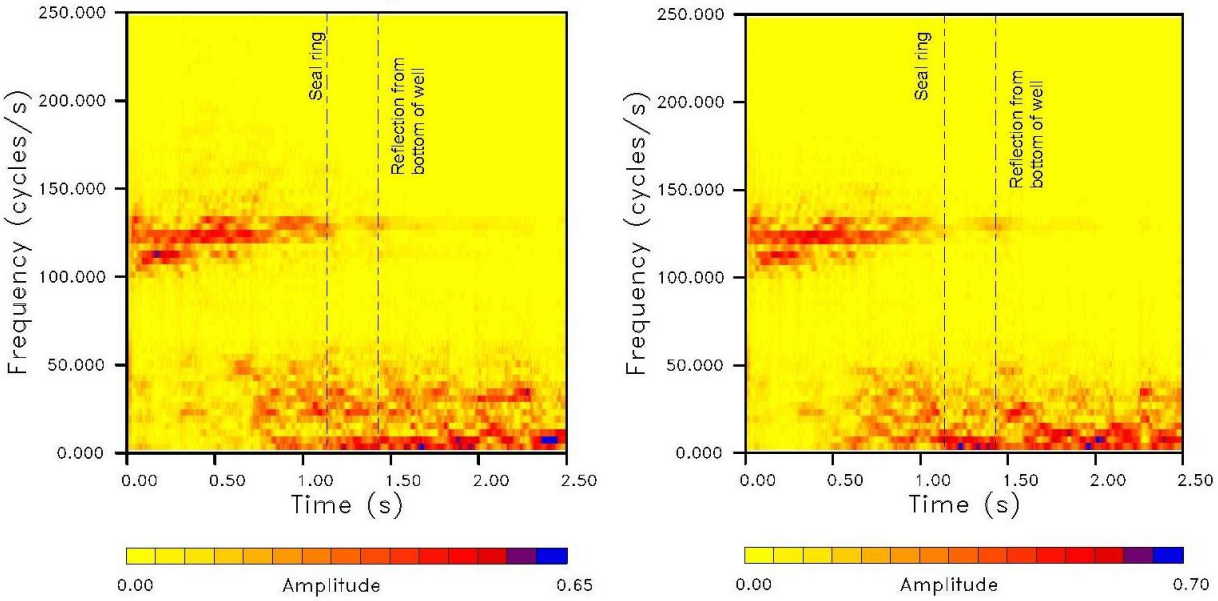

Figure 9. Time-frequency decomposition for a competent or healthy well. The results from two different hammer strikes are shown.

9 we show the results from two different hammer strikes and each contains the secondary arriving energy at the time of the tube wave reflection. Thus, the secondary arriving energy is a robust feature, in spite of the fact that our hammer is not a strong seismic source. That is, regardless of the variations in instrumentation used, all of the results have later arriving high frequency energy that appears at the time of the expected tube wave arrival. This contrasts with the results from the broken wells. When the well is broken there does not seem to be significant later arriving energy. Still, the results from the entire suite of wells, which have a variety of geometries and completion strategies, are complicated and suggest that we would benefit from some additional numerical modeling and improved sources and receivers, as discussed below.

Discussion and Conclusions

There are repeatable differences between healthy and broken wells. These differences are discernable in time-frequency decompositions of the recordings of the seismic response to a hammer blow. The results to date are tentative but warrant continued investigation. Our manual hammer source did not provide sufficient signal strength to reliably produce a definitive visible tube wave reflection for each healthy well. Perhaps this was to be expected because in many, if not most cases the energy had to propagate between one and two kilometers in fairly attenuating environment. It is particularly challenging to propagate energy through the uppermost section of the well due to the gas column that often exists there. By far, the best configuration for generating tube waves is to have source within the well itself, below the top of the fluid column. It is critical to generate disturbances within the fluid column and sources that do so generate strong tube waves and tube wave reflections, as shown for an example from an adjacent California oil field (Figure 10). In areas with high potential for well failure, it should be possible to design a cost-effective permanent source, such as a set of buried piezoelectric sources, either located at depth on the boundary of the well or within the well itself to excite tube waves and to detect and evaluate tube wave reflections.

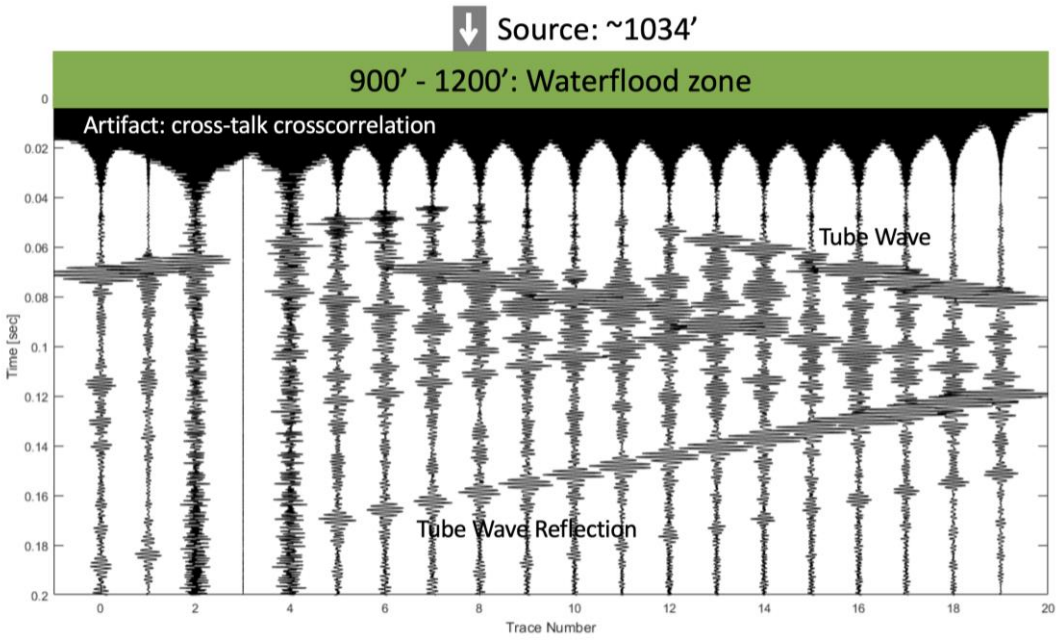

Figure 10. Tube wave and tube wave reflections recorded by a set of geophones within a well.

Dramatic advances in fiber-optic sensing are already impacting well monitoring and will likely revolutionize the evaluation of well integrity (Daley et al. 2013, Dou et al. 2017, Raab et al. 2019). Fiber-optic cables are durable and relatively inexpensive instruments that may extend along the length of the well and record temperature, strain-rate, chemistry, and acoustic wave arrivals in a continuous fashion in time. As noted in Raab et al. (2019),

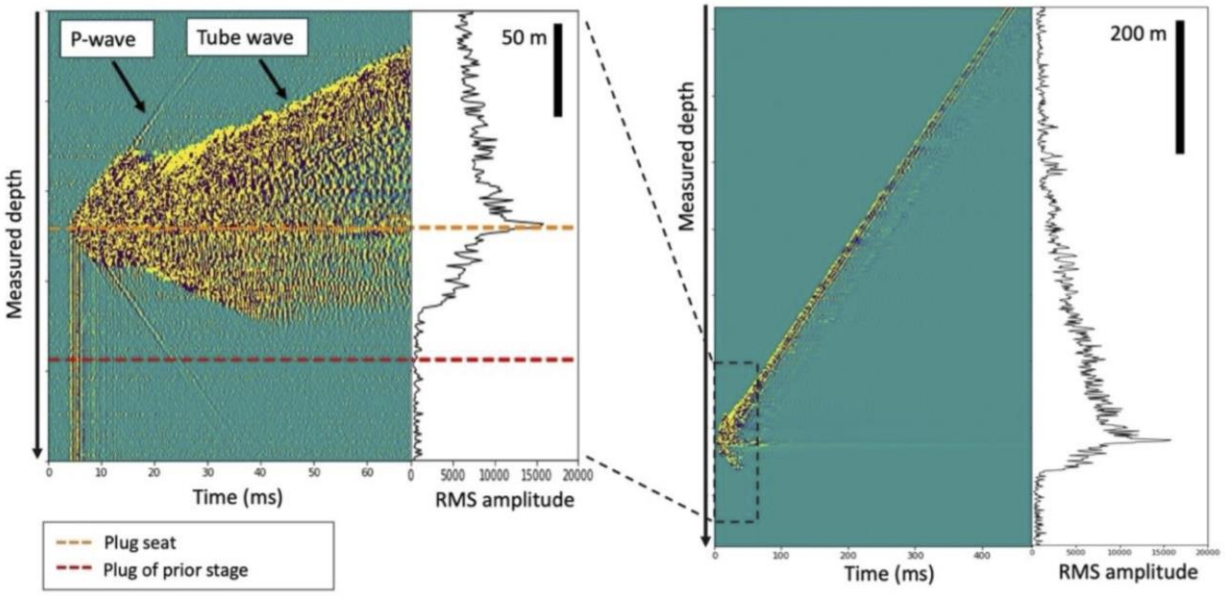

Figure 11. Direct arrivals and tube waves generated by a perforation shot during a hydro-fracturing event. The seismic waves were recorded in an adjacent well. The right panel indicates the attenuation that occurs due to the tube waves encountering previously created hydro-fractures. Figure from Schumann and Jin (2021), used with permission from the Society of Exploration Geophysicists.

tube waves induced by the ambient wavefield are observable on a fiber-optic cable cemented next to an operating well. Thus, fiber-optic cables seem ideally suited for observing waves produced by an active source and can serve as a monitoring system for well integrity. The utility of fiber-optic distributed acoustic sensing (DAS) for well monitoring using tube waves is evident in the recent work of Schumann and Jin (2021) on monitoring hydro-fracture treatments (Figure 11). They found that tube waves generated by perforation shots are clearly visible in DAS records and are very sensitive to the state of the well, being severely attenuated by hydro-fractures from previous treatments. This sensitivity was pointed out several decades ago in a series of papers by various authors (see for example Hornby et al. 1989). Time-lapse DAS monitoring can also be used to detect anomalous behavior in the well, such as the acoustic noise associated with fluid leakage into the surrounding formation (Zhang et al. 2021), and other types of acoustic events associated with fluid injection such as the release of thermal stresses accumulated on borehole tubing or rods used for deployment of tools downhole (Lupis et al, 2021; Figure 12). These events could potentially be used for characterizing and monitoring the formation immediately surrounding the borehole. Low-frequency (< 1 Hz) DAS is also becoming a popular tool for hydraulic fracturing monitoring and could potentially be used to detect well breakage (e.g. Jin and Roy, 2017). In addition to seismic and acoustic monitoring, the temperature sensing capacity of a fiber optic cable can be used to detect flow due to leakage from the well, augmenting information provided by the monitoring of tube waves on well integrity (Zhang et al. 2021).

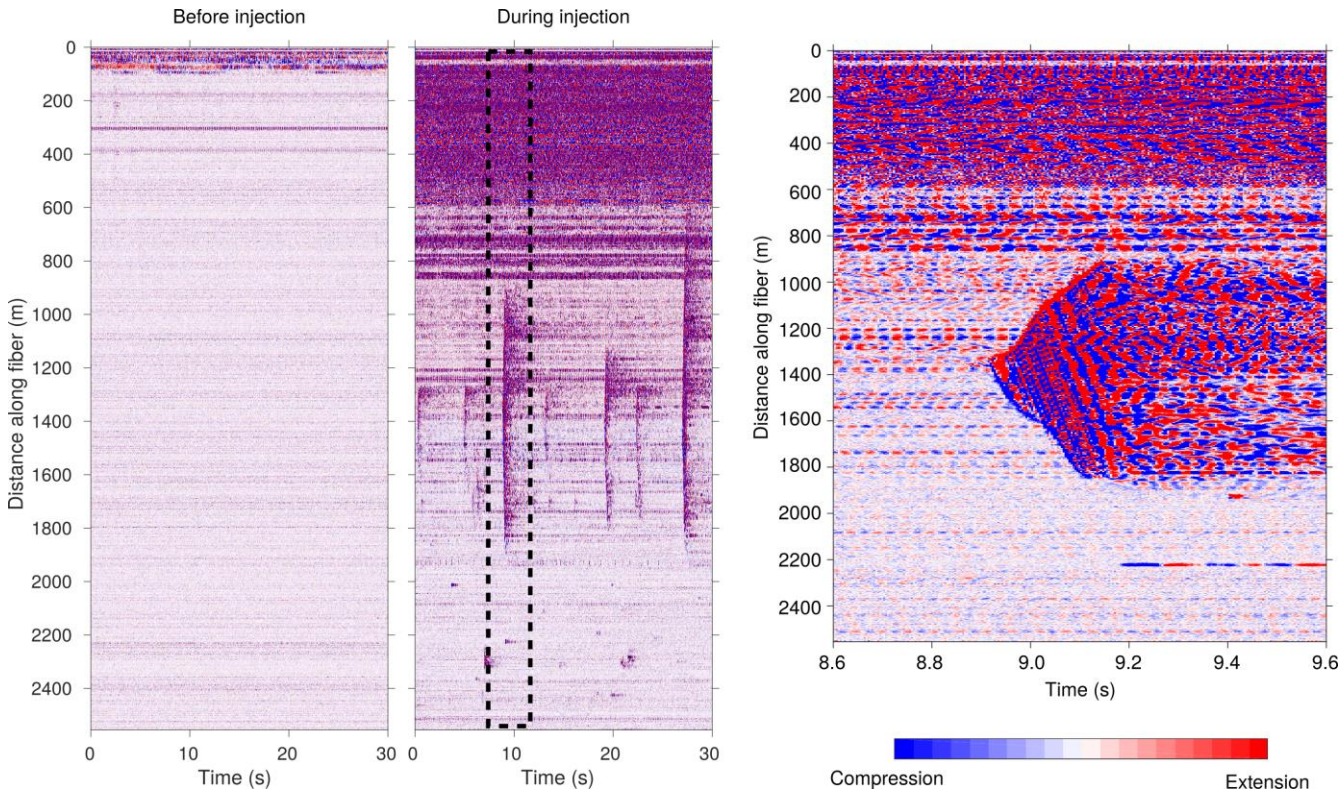

Figure 12. Distributed Acoustic Sensing (DAS) noise records acquired along a well in an underground gas storage facility before and during gas injection (Zhang et al., 2021). Fiber-optic cable is attached to the well tubing. Note noise bursts originate approximately half-way down the well during gas injection. Dashed-line box in the middle panel indicates the enlarged section of the seismic record shown in the right panel, which shows the detail of one of these noise bursts. These events are likely related to the release of thermal stress accumulated on the tubing (Lupis et al. 2021).

Long term monitoring will involve repeated surveys and the extraction of time-lapse variations in the response of the well. Repeated, semi-permanent monitoring of changes in the response of a well should allow detection of progressive well deformation and very subtle variations in well response. This process should be fairly sensitive to changes in the conditions of the well because we can reference the changes to the initial state of the well, thus removing some of the effects of variable well construction. This will be the topic of a future investigation.

Acknowledgements

This work was supported by Chevron and the U.S. Department of Energy under contract DE-AC02-05-CH11231.

References

Daley, T. M., Freifeld, B. M.,and Ajo-Franklin, J. B et al. (2013). Field testing of fiber-optic distributed acoustic sensing (DAS) for subsurface seismic monitoring, The Leading Edge, 32, 6, 699-706, https://doi.org/10.1190/tle32060699.1.

Dou, S., Lindsey, N., Wagner, A. M., et al. (2017). Distributed acoustic sensing for seismic monitoring of the near surface: A traffic-noise interferometry case study, Scientific Reports, 7, 11620. https://doi.org/10.1038/s41598-017-11986-4.

Hornby, B. E., Johnson, D. L., Winkler, K. W., and Plumb, R. A. (1989). Fracture evaluation using reflected Stoneley-wave arrivals, Geophysics, 54, 1274-1288.

Jackson, R. B. (2014). The integrity of oil and gas wells, Proceedings of the National Academy of Sciences, 111, 30, 10902-10903. https://doi.org/10.1073/pnas.1410786111

Jin, G., Roy, B. (2017). Hydraulic-fracture geometry characterization using low-frequency DAS signal, The Leading Edge, 36 (12), 962-1044.

Lupis, M.P., Schölderle, F., Reinsch, T., Wollin, C., Krawczyk, C.M., Pfang, D., Zosseder, K. (2021.) Dynamic motion monitoring of a 3.6 km long steel rod in a borehole during cold-water injection with distributed fiber-optic sensing, Solid Earth Discussions, 2021, https://doi.org/10.5194/se-2021-63

Raab, T., Reinsch, T., Aldaz Cifuentes, S. R., and Henninges, J. (2019). Real-time well-integrity monitoring using fiber-optic distributed acoustic sensing, SPE Journal, 24, 1997-2009.

Schumann, H., and Jin, G. (2021). Near-wellbore hydraulic fracture connectivity inferred by tube waves in DAS perf shot records, First International Meeting for Applied Geoscience and Energy, Society of Exploration Geophysicists, 357-361. Doi:10.1190/segam2021-3582962.1

Simsek, E., and Sinha, B. K. (2008). Estimation of borehole ellipticity using cross-dipole dispersions, Society of Exploration Geophysicists Annual Meeting, Las Vegas.

Sinha, B., and Kostek, S. (1996). Stress-induced azimuthal anisotropy in borehole flexural waves, Geophysics, 61, 1899-1907.

Zhang, Y., Oldenburg, C. M., Zhou, Q., Pan, L., Freifeld, B. M., Jeanne, P., Rodriguez Tribaldos, V., and Vasco, D. W. (2021). Advanced monitoring and simulation of underground gas storage risk management, J. of Petrol. Science and Eng., https://doi.org/10.1016/j.petrol.2021.109763.